 Related Commentary, page 1688

Extracellular matrix proteases contribute to progression of pelvic organ prolapse in mice and humans

Madhusudhan Budatha,[1] Shayzreen Roshanravan,[2] Qian Zheng,[1] Cecilia Weislander,[2] Shelby L. Chapman,[1] Elaine C. Davis,[3] Barry Starcher,[4] R. Ann Word,[2] and Hiromi Yanagisawa[1]

[1]Department of Molecular Biology and [2]Department of Obstetrics and Gynecology, University of Texas Southwestern Medical Center, Dallas, Texas, USA. [3]Department of Anatomy and Cell Biology, McGill University, Montreal, Quebec, Canada. [4]Department of Biochemistry, University of Texas Health Center, Tyler, Texas, USA.

Pelvic organ prolapse (POP) is a common condition affecting almost half of women over the age of 50. The molecular and cellular mechanisms underlying this condition, however, remain poorly understood. Here we have reported that fibulin-5, an integrin-binding matricellular protein that is essential for elastic fiber assembly, regulated the activity of MMP-9 to maintain integrity of the vaginal wall and prevented development of POP. In murine vaginal stromal cells, fibulin-5 inhibited the β_1 integrin–dependent, fibronectin-mediated upregulation of MMP-9. Mice in which the integrin-binding motif was mutated to an integrin-disrupting motif (*Fbln5*$^{RGE/RGE}$) exhibited upregulation of MMP-9 in vaginal tissues. In contrast to fibulin-5 knockouts (*Fbln5*$^{-/-}$), *Fbln5*$^{RGE/RGE}$ mice were able to form intact elastic fibers and did not exhibit POP. However, treatment of mice with β-aminopropionitrile (BAPN), an inhibitor of matrix cross-linking enzymes, induced subclinical POP. Conversely, deletion of *Mmp9* in *Fbln5*$^{-/-}$ mice significantly attenuated POP by increasing elastic fiber density and improving collagen fibrils. Vaginal tissue samples from pre- and postmenopausal women with POP also displayed significantly increased levels of MMP-9. These results suggest that POP is an acquired disorder of extracellular matrix and that therapies targeting matrix proteases may be successful for preventing or ameliorating POP in women.

Introduction

Pelvic organ prolapse (POP) is characterized by abnormal protrusion of female pelvic organs involving the uterus, bladder, and vagina (reviewed in refs. 1–3). Epidemiologic studies indicate that (a) vaginal birth, aging, and increased body mass index are major risk factors for the development of POP and (b) more than 1 pathology may be involved to exhibit full anatomical loss of support. Although approximately 11% of women have surgery for POP or urinary incontinence in their lifetimes (4), to date, effective therapies to prevent progression of POP have not been established, thereby imposing profound social and financial burden to affected individuals (3).

Despite a difference in anatomical position of pelvic organs relative to the body axis and pelvic floor, rodent models of POP have provided important tools to study underlying mechanisms of prolapse. In contrast to an observation that rectal prolapse is frequently associated with the presence of chronic inflammatory bowel disease (5), POP has been found in animals with defective ECM proteins, including fibulin-3, fibulin-5, and lysyl oxidase-like–1 (LOXL-1) (an enzyme that predominantly catalyzes cross-linking of elastin) (6–8). Interestingly, these proteins are abundantly expressed in the vaginal wall and involved in synthesis and assembly of elastic fibers. It is also known that uterosacral ligaments support the vaginal wall and that Hoxa11 is essential for formation of uterosacral ligaments in mice (9). *Hoxa11*-deficient mice exhibit increased mobility of the uterus; however, POP was not reported. Hence, it has been proposed that intact elastic fibers are required for maintenance of vaginal wall support. The specific role of elastic fibers in this process is not clear; however, because upregulation of matrix proteases in the vaginal wall either precedes or coincides with POP in these mice with elastic fiber deficiencies, a potential link between elastic fibers, matrix degradation, and development of POP is suggested (10). The precise mechanisms that regulate matrix proteases in the vaginal wall, whether or not a tissue-specific mechanism exists, and how these mechanisms affect the integrity of the vaginal wall have not been fully elucidated.

Fibulins are a family of matricellular modular proteins characterized by the presence of repeated calcium-binding EGF-like motifs and a C-terminal fibulin domain and are involved in structural stability of the basement membrane and formation of elastic fibers (reviewed in refs. 11 and 12). Among fibulins, fibulin-5 possesses potent elastogenic functions (reviewed in ref. 13). It was suggested that fibulin-5 organizes elastic fiber assembly machinery on microfibrillar scaffolds by serving as an adaptor protein to structural components of elastic fibers and cross-linking enzymes, including elastin, fibrillin-1, emilin-1, and LOXL-1 (8, 14–19). Systemic elastic fiber phenotypes are evident early in life in *Fbln5*$^{-/-}$ mice without overt inflammatory cell infiltration, suggesting that the underlying defect is primarily a developmental defect in elastogenesis rather than a progressive destruction of elastic fibers (14). Interestingly, however, the POP phenotype in *Fbln5*$^{-/-}$ mice is not observed until after puberty and is preceded by substantial upregulation of MMP-9 in the vaginal wall (10). In addition, delayed manifestation and progressive worsening of the POP phenotype correlate with aging (7).

Authorship note: Ann Word and Hiromi Yanagisawa are co-senior authors.
Conflict of interest: The authors have declared that no conflict of interest exists.
Citation for this article: *J Clin Invest.* 2011;121(5):2048–2059. doi:10.1172/JCI45636.

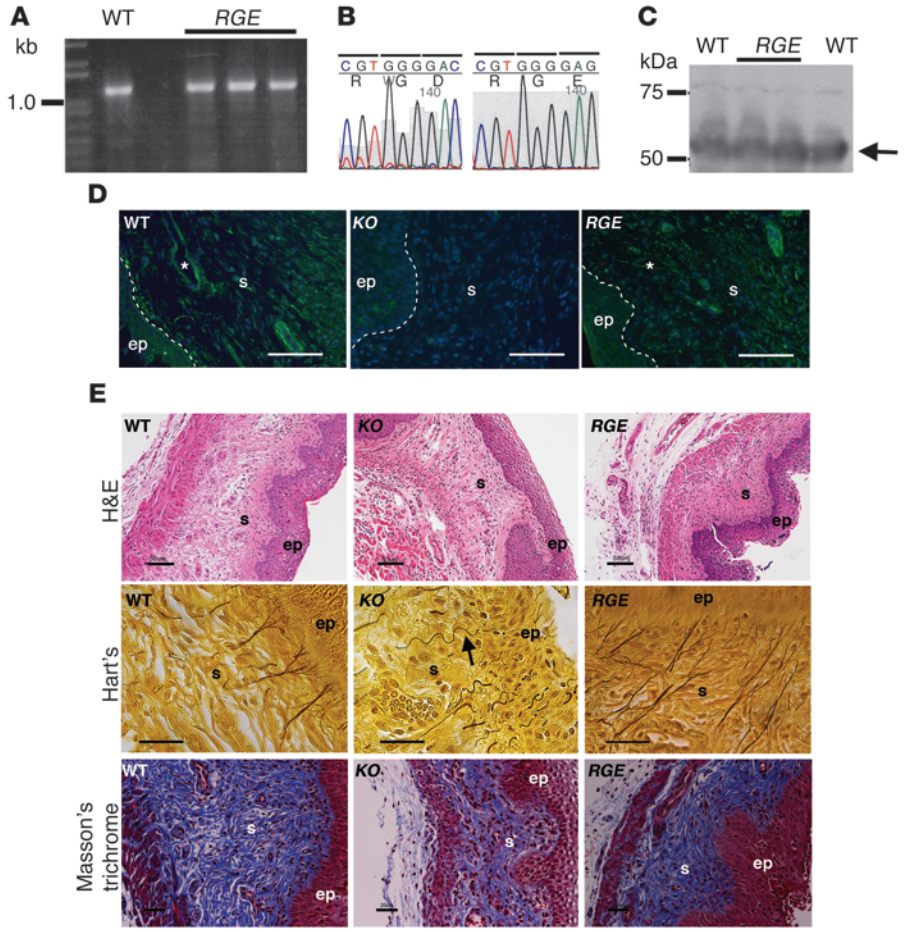

Figure 1
Characterization of *Fbln5*$^{RGE/RGE}$ (*RGE*) mice. (**A**) RT-PCR of *Fbln5* from WT and *RGE* kidney mRNA. (**B**) Sequencing confirms a successful mutation of D56E. (**C**) Western blot analysis showing comparable level of fibulin-5 protein in the WT and mutant kidneys. (**D**) Representative fibulin-5 immunostaining in the vagina from WT, *Fbln5*$^{-/-}$ (KO), and *RGE* mice. Note strong fibulin-5 expression in the vaginal stroma in WT and RGE mice. Asterisks indicate vessels. Scale bars: 50 μm. (**E**) Histological analysis of vaginal wall from WT, KO, and *RGE* mice at 4 weeks of age stained with H&E, Hart's, or Masson's trichrome. Numerous long branching elastic fibers are seen in WT and *RGE* vagina, whereas abnormal elastic fibers are present in KO mouse (arrow). Scale bars: 50 μm (H&E); 20 μm (Hart's and Masson's trichrome). ep, epithelium; s, stroma.

Fibulin-5 contains a motif that is not shared by other fibulins: an evolutionally conserved arginine-glycine-aspartic acid (RGD) sequence known to mediate binding to cell surface integrin receptors (20). Binding of the RGD-containing ECM proteins to integrins transmits environmental cues to cells, which activates intracellular signaling and induces cytoskeletal changes, as well as upregulates metalloproteases (ref. 21, reviewed in ref. 22, and ref. 23). The RGD in fibulin-5 has been previously shown to facilitate adhesion of endothelial cells and inhibit transcription of MMP-7 in breast cancer cells (24, 25). We have also shown that the RGD-dependent fibulin-5–integrin interaction controls pancreas tumor growth by regulating ROS production and tumor angiogenesis (26). Although it is initially speculated that the binding of fibulin-5 to integrins is necessary for tethering of newly synthesized elastic fibers to surrounding cells, the exact role of the RGD motif in elastic fiber assembly has not been elucidated. Therefore, we sought to determine the biological function of the RGD motif of fibulin-5, focusing on pathogenesis of POP. We hypothesized that disruption of the RGD motif would result in impaired elastic fiber assembly and dysregulation of MMP-9 in connective tissues of the pelvic floor.

Here, we demonstrate a dual role of fibulin-5 in regulation of matrix homeostasis in the vaginal wall. First, we show that fibulin-5 facilitates assembly of elastic fibers independent of integrins and that this fibulin-5–mediated elastogenesis is crucial for pelvic organ support. Second, we present evidence that fibulin-5 inhibits MMP-9 in an integrin-dependent manner. This function of fibulin-5 is important in the pathogenesis of POP because abnormal elastic fibers alone, without MMP-9 activation, are insufficient for full manifestation of the disease. Thus, fibulin-5 strengthens the vaginal wall and protects from prolapse development. Our finding that genetic ablation of MMP-9 significantly attenuated progression of POP in vivo provides the foundation for development of novel preventative and therapeutic strategies for POP in women.

Results

Generation and characterization of Fbln5$^{RGE/RGE}$ *knockin mice*. To test the hypothesis that RGD-dependent fibulin-5–integrin interaction is required for assembly and organization of elastic fibers in vivo, we generated a mouse carrying homozygous alleles of mutant *Fbln5* in which the RGD motif in exon 4 was replaced with an inactive RGE (D56E, *Fbln5*^{RGE}) by homologous recombination (Supplemental Figure 1; supplemental material available online with this article; doi:10.1172/JCI45636DS1). Two ES cell clones were obtained, which gave germline transmission; and homozygous mice were born with the expected Mendelian frequency. The transcript levels from D56E alleles were comparable to those from WT alleles (Figure 1A), and sequencing of reverse transcribed mRNA from kidney confirmed that correct mutation was achieved in *Fbln5*$^{RGE/RGE}$ mice (Figure 1B). We also confirmed that protein levels were comparable between WT and *Fbln5*$^{RGE/RGE}$ mice by Western blot analysis using kidney extracts (Figure 1C). Surprisingly, elastic fibers were

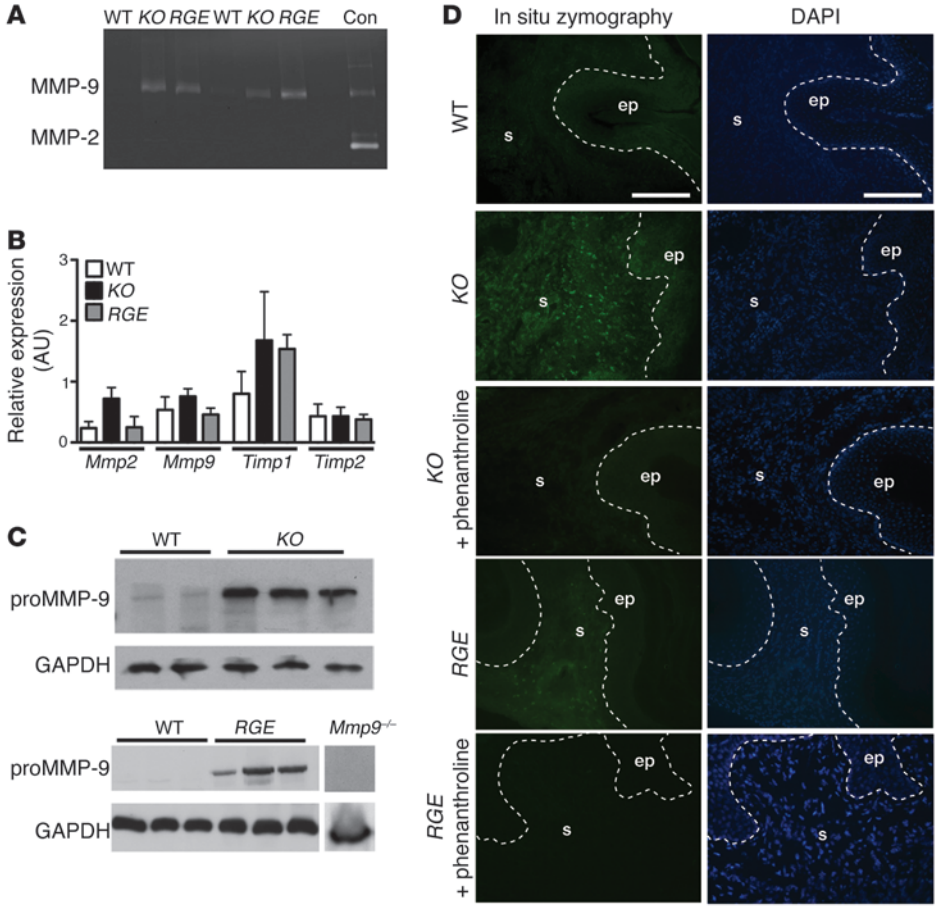

Figure 2
MMP-9 is increased in vaginal tissues from *Fbln5*$^{-/-}$ (KO) and *Fbln5*$^{RGE/RGE}$ (*RGE*) mice. (**A**) Gelatin zymography of vaginal tissues from WT and *Fbln5* mutants. Con, conditioned media harvested from WT mouse vaginal stromal cells stimulated with TNF-α, showing MMP-9 and MMP-2. (**B**) qPCR using vaginal mRNA from WT (white bars), KO (black bars), and *RGE* (gray bars) mice. mRNA was expressed relative to that of β_2-microglobulin, and data represent mean ± SEM of 3–4 mice in each group. No statistical significance was obtained. (**C**) Western blot analysis using anti–MMP-9 proenzyme antibody. Note strong proMMP-9 expression in vaginal tissues from KO (upper gel) and *RGE* (lower gel) mice. *Mmp9*$^{-/-}$ served as negative control, and GAPDH was detected as loading control. (**D**) In situ zymography of 10-μm vagina sections from young (6 weeks) WT, KO, and *RGE* mice. Nuclei are stained with DAPI. Gelatinolytic activity was predominantly detected in the KO and *RGE* vaginal stroma after incubation with DQ gelatin. Limited activity was detected in WT vagina. Phenanthroline, an MMP inhibitor, completely inhibited gelatinolytic activity in mutant vagina. Scale bars: 50 μm.

normal in the aorta, skin, lungs, and coronary arteries by histological analysis (Supplemental Figure 2A). Electron microscopic analysis of the aorta at P5 and P90 showed normal elastic laminae and well-formed connections between elastic fibers and smooth muscle cells in *Fbln5*$^{RGE/RGE}$ mice (Supplemental Figure 2B). Biochemical analysis of desmosine, an elastin-specific cross-link, in the skin, aorta, and lung showed comparable levels between WT and *Fbln5*$^{RGE/RGE}$ mutant mice (Supplemental Figure 2C).

Fbln5$^{RGE/RGE}$ *knockin mice rescue the POP phenotype.* *Fbln5*$^{RGE/RGE}$ mice were healthy and indistinguishable from WT littermates. Fertility and fecundity appeared normal. Importantly, prolapse was not observed in *Fbln5*$^{RGE/RGE}$ knockin mice (~200 females), and aging up to 1 year or repeated vaginal deliveries did not induce the prolapse phenotype. Next, we used immunohistochemistry to localize expression and distribution of fibulin-5 in the vaginal wall of *Fbln5*$^{RGE/RGE}$ mice at 6 weeks of age. Fibulin-5 was localized to the stroma of the vaginal wall connective tissues and around vessel walls in both WT and *Fbln5*$^{RGE/RGE}$ vagina but not in the *Fbln5*$^{-/-}$ vagina (Figure 1D). H&E staining showed similar tissue architecture in all genotypes (Figure 1E). Hart's staining revealed long elastic fibers extending perpendicularly from the lamina propria branching in a candelabra-like pattern immediately beneath the basal layer of the vaginal epithelium in both WT and *Fbln5*$^{RGE/RGE}$ mice (Figure 1E). In contrast, elastic fibers were short, thick and tortuous and without branching in vaginal tissues from young *Fbln5*$^{-/-}$ mice. Masson's trichrome staining showed normal collagen fibers in *Fbln5*$^{RGE/RGE}$ vagina (Figure 1E). These data indicate that RGD-dependent integrin binding of fibulin-5 is not required for elastic fiber formation in vivo. Further, generation of mice with mutated fibulin-5 results in rescue of the prolapse phenotype.

MMP-9 is increased in vaginal tissues from *Fbln5*$^{-/-}$ *and* *Fbln5*$^{RGE/RGE}$ *mice.* Previously, we reported that POP does not develop until later in life in *Fbln5*$^{-/-}$ mice and is preceded by increased MMP-9 in the vaginal wall (7, 10). To investigate the potential involvement of integrin ligation in MMP-9 upregulation, we examined MMP-9 levels in the *Fbln5*$^{RGE/RGE}$ vagina by gelatin zymography. MMP-9 was increased significantly in vaginal tissues from *Fbln5*$^{RGE/RGE}$ mice, which was comparable to levels in the *Fbln5*$^{-/-}$ vagina (Figure 2A). Interestingly, we did not detect differences in MMP-9 or MMP-2 between WT and *Fbln5*$^{RGE/RGE}$ mice in other elastogenic tissues, including the aorta and skin (data not shown). Incubation with aminophenylmercuric acetate (APMA), a chemical activator of MMP-9, revealed that the increased MMP-9 predominantly consisted of the proform (Supplemental Figure 3). Transcript levels of *Mmp9*, *Mmp2*, and their endogenous inhibitors, *Timp1* and *Timp2*, were not statistically different among WT, *Fbln5*$^{-/-}$, and *Fbln5*$^{RGE/RGE}$ vaginas, suggesting that the increased MMP-9 reflected posttranscriptional regulation (Figure 2B). We also confirmed the increase of MMP-9 in the vaginal tissues by Western blot analysis using an anti–MMP-9 proenzyme antibody (Figure 2C and ref. 27). Strong expression of proMMP-9 was observed in vaginal tissues from *Fbln5*$^{-/-}$ and *Fbln5*$^{RGE/RGE}$ mice but not from WT mice. Hence, proMMP-9 is increased in the vaginal wall of *Fbln5*$^{RGE/RGE}$ animals despite normal elastic fibers and the absence of POP.

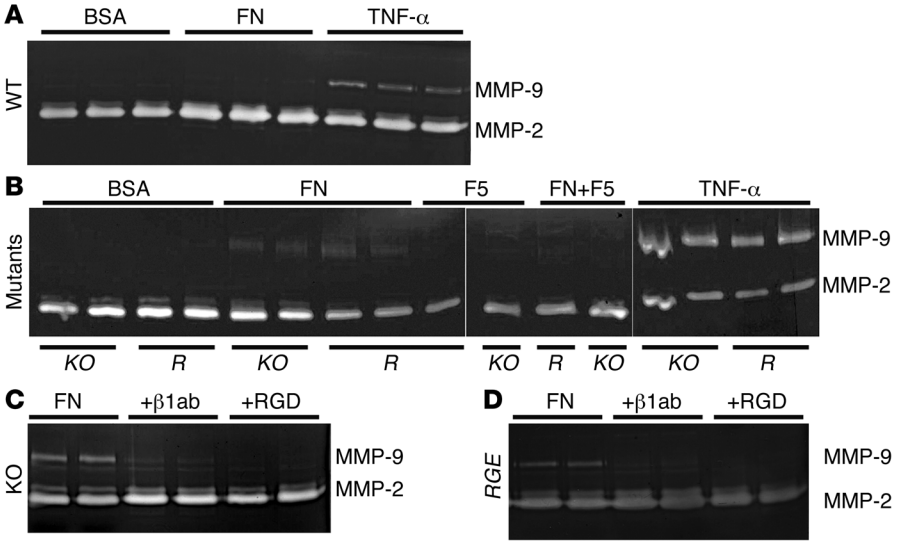

Figure 3

Gelatin zymography using conditioned media from primary vaginal stromal cells. (**A**) Conditioned media were harvested from WT cells after 24 hours of stimulation. Fibronectin (FN) did not alter gelatinolytic activity in WT cells. TNF-α was used as positive control for MMP-9 induction. (**B**) *Fbln5*$^{-/-}$ (KO) or *Fbln5*$^{RGE/RGE}$ (R) cells were incubated with FN, fibulin-5 (F5), or both simultaneously (FN+F5). Note a marked upregulation of MMP-9 after fibronectin stimulation in mutant cells. Whereas fibulin-5 alone showed no effects, fibulin-5 inhibited fibronectin-induced upregulation of proMMP-9. (**C** and **D**) Incubation with β_1 integrin–blocking antibody or RGD peptides inhibited fibronectin-induced upregulation of MMP-9 in KO (**C**) and *RGE* (**D**) stromal cells. Experiments were performed 4 times using independent primary cell preparations. In **B**, the last 7 lanes were run on the same gel but were noncontiguous.

To identify the cell type responsible for the increased MMP-9, we performed in situ zymography using DQ gelatin as substrate. Intense fluorescence was observed throughout the stroma of the vaginal wall in the *Fbln5*$^{-/-}$ and *Fbln5*$^{RGE/RGE}$ vagina, and this activity was completely blocked by phenanthroline, an inhibitor of MMP (Figure 2D). Increased MMP-9 activity did not appear to be predominantly from macrophages because the number of CD68-positive cells was comparable between WT and *Fbln5*$^{-/-}$ vaginal tissues (data not shown). These data indicate that fibulin-5 regulates MMP-9 expression at a posttranscriptional level via the RGD motif and that this regulation takes place in a cell- and tissue-specific manner.

Fibulin-5 controls MMP-9 via its RGD motif in vaginal stromal cells. Fibulin-5 has been shown to bind subsets of cell surface integrins, including $\alpha_v\beta_3$, $\alpha_v\beta_5$, $\alpha_4\beta_1$, and $\alpha_5\beta_1$, and mediate substrate binding of vascular cells (28, 29). Interestingly, binding of fibulin-5 to $\alpha_5\beta_1$ integrin, a primary fibronectin receptor, blocks fibronectin-mediated activation of β_1 integrin, actin fiber formation, and focal adhesions (29). Since fibronectin has been shown to upregulate proMMP-9 (30), we hypothesized that fibulin-5 fine-tunes ECM-mediated signaling by competing with signal-transducing ECM for integrin ligation and thus negatively regulates fibronectin- and integrin-mediated upregulation of MMP-9 in the vaginal wall. To test this hypothesis, we first determined whether fibronectin is a relevant ECM in the vaginal wall by immunostaining. Strong fibronectin immunoreactivity was observed in the vaginal stroma of WT, *Fbln5*$^{-/-}$, and *Fbln5*$^{RGE/RGE}$ vaginas (Supplemental Figure 4A). Next, we established primary vaginal stromal cells from P14–P21 WT and mutant mice, in which hormonal effects were negligible before sexual maturity. Immunostaining of WT, *Fbln5*$^{-/-}$, and *Fbln5*$^{RGE/RGE}$ stromal cells with α–smooth muscle (α-SM) actin and vimentin confirmed that these cells were of mesenchymal origin (Supplemental Figure 4B and Supplemental Table 1). In contrast, staining with cytokeratin and CD68, markers for epithelial cells and activated macrophages, respectively, was negative, thus validating the purity of stromal cells. We then investigated integrin profiles by RT-PCR and confirmed that $\alpha_5\beta_1$ integrin was expressed in WT, *Fbln5*$^{-/-}$, and *Fbln5*$^{RGE/RGE}$ stromal cells. No difference was observed in the expression of major integrins among genotypes (Supplemental Figure 4C).

Using vaginal stromal cells in the first passage, we determined the effect of fibronectin on MMP-9 levels by gelatin zymography. Stimulation of WT cells with BSA (50 μg/ml) or fibronectin (50 μg/ml) for 24 hours did not upregulate MMP-9, whereas stimulation with TNF-α (10 ng/ml) was sufficient to induce MMP-9 (Figure 3A). In contrast, stimulation of *Fbln5*$^{-/-}$ or *Fbln5*$^{RGE/RGE}$ cells with fibronectin, but not BSA, fibulin-5, or laminin (data not shown), resulted in marked increases in MMP-9. Fibronectin-mediated upregulation of MMP-9 was inhibited by simultaneous incubation with fibulin-5, suggesting that fibulin-5 blocks the function of fibronectin in the mutant cells (Figure 3B). To determine whether MMP-9 upregulation is mediated by β_1 integrin, we treated *Fbln5*$^{-/-}$ and *Fbln5*$^{RGE/RGE}$ cells with an integrin β_1 integrin–blocking antibody (clone Ha2/5) and then stimulated the cells with fibronectin. While incubation with a nonspecific IgG did not affect MMP-9 levels (Supplemental Figure 5), the β_1 integrin–blocking antibody clearly suppressed fibronectin-mediated MMP-9 upregulation in *Fbln5*$^{-/-}$ and *Fbln5*$^{RGE/RGE}$ cells (Figure 3, C and D). Incubation of fibronectin with RGD peptides also decreased MMP-9 levels, indicating that RGD-mediated fibronectin-integrin ligation is important for the MMP-9 increase (Figure 3, C and D). MMP-2 levels, in contrast, were unchanged by fibronectin stimulation. Taken together, these in vitro data show that (a) MMP-9 is upregulated by fibronectin via the β_1 integrin, and (b) fibulin-5 inhibits fibronectin-mediated MMP-9 upregulation in an RGD-dependent manner.

ROS upregulates MMP-9 levels in Fbln5$^{-/-}$ *and Fbln5*$^{RGE/RGE}$ *stromal cells.* We have recently shown that ligation of fibronectin with β_1 integrin leads to enhanced generation of ROS in *Fbln5*$^{-/-}$ or *Fbln5*$^{RGE/RGE}$ mouse embryonic fibroblasts (26). Since ROS is known to increase proMMP-9 levels and to convert proMMP-9 to active MMP-9 by a nonproteolytic mechanism (30, 31), we reasoned that upregulation of MMP-9 (both pro– and active) in the *Fbln5*$^{-/-}$ and *Fbln5*$^{RGE/RGE}$ vaginal wall may be related to concomitant production of ROS and that ROS may be an upstream regulator of MMP-9 in mutant stromal cells. To test this hypothesis, we first examined ROS levels in the vaginal wall of young (6 week) *Fbln5*$^{-/-}$ and

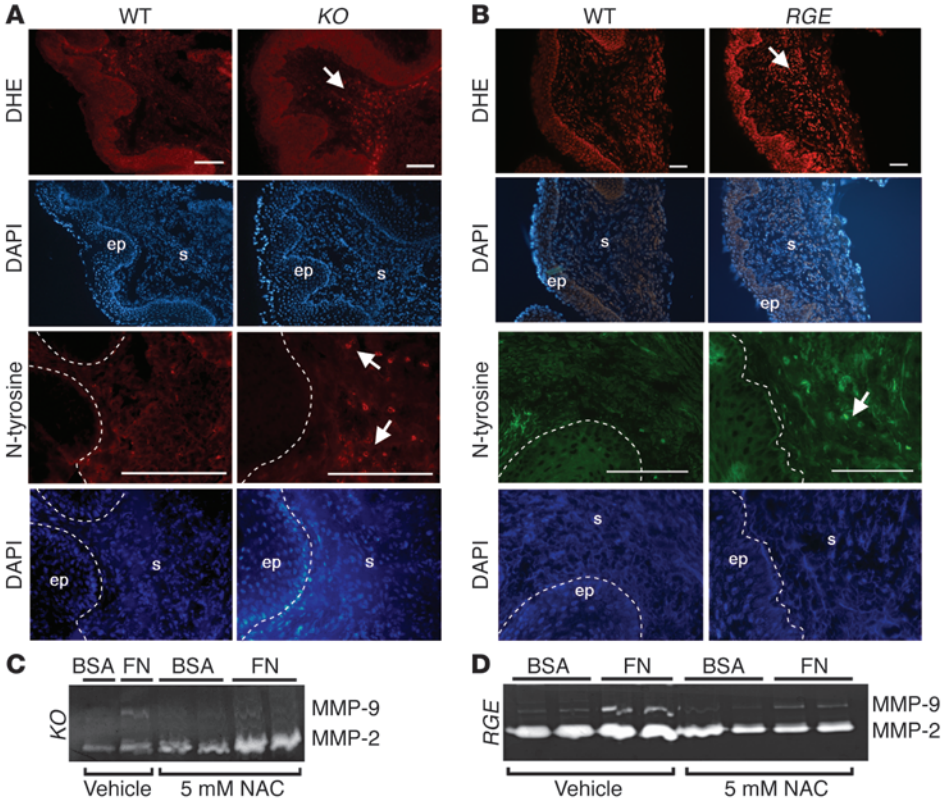

Figure 4
Increased oxidative stress in KO and *RGE* vaginal tissues. (**A** and **B**) In situ detection of superoxide production with DHE and anti–N-tyrosine in vaginal tissues from (**A**) KO ($n = 3$) and (**B**) *RGE* ($n = 3$) mice at 4 weeks of age in comparison with WT mice ($n = 3$). Corresponding DAPI staining images are shown. Note an increase in ROS levels in the vaginal stroma in KO and *RGE* mice (arrows). Scale bars: 100 μm. (**C** and **D**) NAC inhibits fibronectin-induced MMP-9 upregulation in KO (**C**) and *RGE* (**D**) vaginal stromal cells. Experiments were performed 4 times using independent primary cell preparations.

Fbln5$^{RGE/RGE}$ mice, in which POP has not developed. Incubation with dihydroethidium (DHE) showed an increase in fluorescence intensity in the vaginal stroma of *Fbln5*$^{-/-}$ and *Fbln5*$^{RGE/RGE}$ mice compared with WT (Figure 4, A and B). The fact that presence of mutant fibulin-5 (RGE) did not rescue the increase in ROS levels indicates that it is not simply due to a lack of tethering ability of SOD3 because the SOD3-binding domain is located at the at the C terminus of fibulin-5 and is intact in *Fbln5*$^{RGE/RGE}$ mutants (32). Immunostaining with antinitrotyrosine, which is formed by nitrosylation of tyrosine by potent oxidant peroxynitrite, also showed increased staining in the vaginal stroma of *Fbln5*$^{-/-}$ and *Fbln5*$^{RGE/RGE}$ compared with WT mice (Figure 4, A and B). Next, we examined the causal relationship between ROS and MMP-9 in *Fbln5* mutant stromal cells. Stimulation of *Fbln5*$^{-/-}$ and *Fbln5*$^{RGE/RGE}$ cells with fibronectin in the presence of N-acetyl cysteine (NAC) (5 mM), an antioxidant and ROS scavenger, resulted in marked decreases in MMP-9 levels, whereas the vehicle control showed no effects (Figure 4, C and D). These results suggest that increased oxidative stress in the absence of fibulin-5–integrin interaction may be responsible, in part, for upregulation of MMP-9 in the mutant vaginal wall.

Inhibition of LOX activity confers susceptibility to POP in Fbln5$^{RGE/RGE}$ *mice*. Although MMP-9 is increased substantially in the vaginal wall of *Fbln5*$^{RGE/RGE}$ mice, it appears that normal elastic fiber assembly protects these animals from prolapse development. In women, POP is associated with aging (33). Since expression of elastic fiber–associated proteins decreases with age (34), it is conceivable that a loss of elastic fiber–associated proteins in connective tissues of the pelvic floor with aging may disrupt an optimal balance between synthesis and degradation of vaginal elastic fibers and lead to POP. To test this concept, we treated mice with β-aminopropionitrile (BAPN), a potent irreversible inhibitor of LOX (35), to block de novo synthesis of elastic fibers and mature cross-linked collagen. WT ($n = 3$), *Fbln5*$^{RGE/+}$ ($n = 6$), and *Fbln5*$^{RGE/RGE}$ ($n = 7$) mice were treated from 3 weeks of age (0.8% in drinking water, ad libitum) and mouse pelvic organ quantification (MOPQ) examinations were conducted weekly from 8 to 25 weeks of age. Since we did not detect statistically significant differences between WT and *Fbln5*$^{RGE/+}$ heterozygotes at any time point, we combined these 2 groups (presented as control animals in Figure 5A). During the observation period, advanced prolapse (≥ stage 2) was not detected in any of the mice. Although this concentration of BAPN treatment resulted in increased perineal body length in both control and *Fbln5*$^{RGE/RGE}$ mice, changes in *Fbln5*$^{RGE/RGE}$ animals were more dramatic (Figure 5A). To confirm the effect of BAPN on collagen and elastic fiber formation, we quantified desmosine and hydroxyproline (HP) levels in vaginal tissues from control and BAPN-treated mice. BAPN treatment resulted in significant decreased HP content of the vaginal wall, and desmosine content also tended to be decreased (Figure 5B). Disruption of elastic fibers or reduction of collagen fibers in the vaginal wall of BAPN-treated *Fbln5*$^{RGE/RGE}$ animals, however, was not detected at the light microscopy level (data not shown). These results suggest that disruption of de novo assembly of elastin and collagen fibers by BAPN confers susceptibility to subclinical prolapse in *Fbln5*$^{RGE/RGE}$ animals.

Genetic ablation of Mmp9 in Fbln5$^{-/-}$ *mice attenuates prolapse formation*. To further investigate the relevance of MMP-9 in prolapse development in vivo, we analyzed the ontogeny of MMP-9 activation in the vaginal wall of *Fbln5*$^{-/-}$ mice during postnatal life. Whereas MMP-9 was increased in the vaginal wall of *Fbln5*$^{-/-}$ mice after P24, MMP-9 was absent in WT animals during this

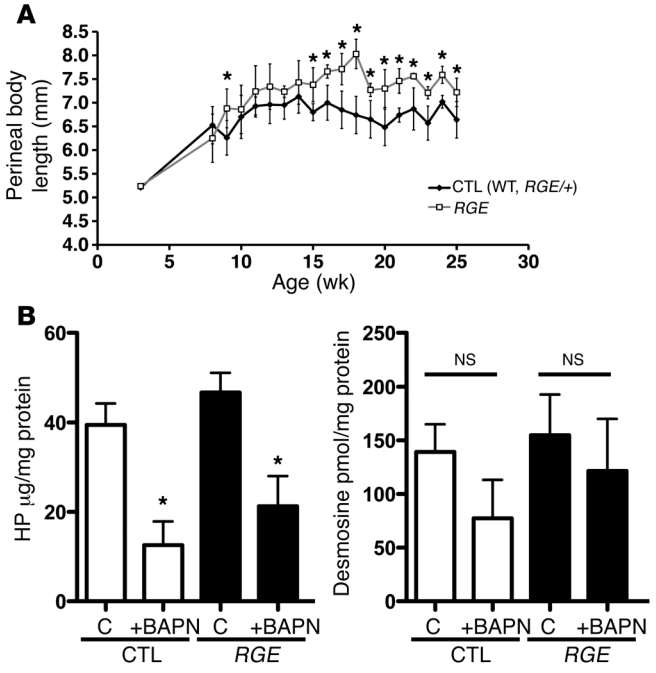

Figure 5
Inhibition of lysyl oxidase unmasks prolapse phenotype in *RGE* mice. (**A**) Control (*Fbln5*$^{+/+}$, $n = 3$; *Fbln5*$^{RGE/+}$, $n = 6$) and *RGE* ($n = 7$) females were treated with BAPN (0.8% in drinking water) from 3 weeks of age until 25 weeks. Perineal body length was measured weekly from 8 weeks of age by examiners blinded to genotype. Although overt prolapse did not develop in *RGE* mice (not shown), BAPN treatment increased perineal body length in the mutants compared with control animals. Data are represented as mean ± SD. *$P < 0.01$. (**B**) Biochemical analyses of HP and desmosine in vaginal tissues from WT and *RGE* mice treated with (+BAPN) or without (C) BAPN. Data are represented as mean ± SEM.

time (Figure 6A). The results indicate that vaginal MMP-9, but not MMP-2, was increased in *Fbln5*$^{-/-}$ mice postnatally during the time of sexual maturity, several weeks prior to the first phenotypic signs of POP (10–12 weeks).

To determine the importance of MMP-9 in the pathophysiology of POP in *Fbln5*$^{-/-}$ mice, we generated mice deficient in both *Mmp9* and *Fbln5* (termed *DKO*). MOPQ examinations were conducted weekly in WT ($n = 23$), *Fbln5*$^{-/-}$*;Mmp9*$^{+/+}$ ($n = 35$), *Fbln5*$^{-/-}$*;Mmp9*$^{+/-}$ ($n = 42$), and DKO ($n = 25$) mice for 1 year (Figure 6B and Supplemental Table 2). The severity and time course of prolapse development were similar in *Fbln5*$^{-/-}$ and *Fbln5*$^{-/-}$*;Mmp9*$^{+/-}$ mice. Prolapse development, however, was ameliorated significantly in DKO animals (Figure 6, B and C). For example, at 36 weeks of age, 96% of *Fbln5*$^{-/-}$*;Mmp9*$^{+/+}$ females developed POP. Prolapse developed in only 42% of DKO females, suggesting that *Mmp9* deficiency rescued the prolapse phenotype in approximately 60% of *Fbln5*$^{-/-}$ animals (Supplemental Table 2). Skin laxity and tortuosity of the aorta were not rescued (data not shown). Next, we determined whether loss of MMP-9 was associated with improvement of elastic fibers or histomorphology of the vaginal wall. Hart's staining of transverse sections of the midvagina of rescued DKO females at 1 year of age revealed marked increases in elastic fiber density in subepithelial vaginal stroma compared with *Fbln5*$^{-/-}$ animals, although each fiber was still short and disrupted (Figure 6D). This is consistent with the quantification of elastic fiber density (Figure 6E). Interestingly, elastic fibers in deep stroma near the muscle layers were comparable between *Fbln5*$^{-/-}$ and DKO mice, indicating that MMP-9–mediated elastic fiber degradation was more prominent in superficial layers near the epithelium and that epithelial-stromal interactions may be important in regulation of MMP-9 in the vaginal wall.

To further evaluate the effect of loss of MMP-9 on morphology of collagen fibers in the vaginal wall, pentachrome and picrosirius red staining were performed. Whereas collagen bundles were thin, irregular, and disrupted in the vaginal wall of *Fbln5*$^{-/-}$ mice, thick and continuous bundles were observed in the DKO vagina (Figure 6D). Quantification of collagen fibers performed on sections stained with picrosirius red was consistent with these data (Figure 6F and Supplemental Figure 6). Taken together, MMP-9 ablation protected from progressive degradation of elastic fibers as well as collagen fibers in the vaginal wall of DKO animals, suggesting that integrity of the ECM is important for prevention of POP in vivo.

MMP-9 upregulation in the vaginal wall of women with POP. Finally, to determine the biological relevance of matrix proteases in human POP, we quantified transcript levels of *MMP9* and *MMP2* in the vaginal muscularis from the anterior vaginal wall apex in premenopausal asymptomatic controls, postmenopausal controls, and 53 women with POP (Supplemental Table 3 and Figure 7A). Expression of *MMP2* and *MMP9* was more likely to be increased in women with POP (particularly postmenopausal women). Next, we performed gelatin zymography using vaginal muscularis from premenopausal women with or without POP (Supplemental Table 4). Since separation of pro– and active MMP-9 is difficult (data not shown), MMP-9 is used to signify total MMP-9 (both pro– and active forms). MMP-9 was increased in the vaginal muscularis of premenopausal women with prolapse compared with controls (Figure 7, B and C). Additional zymograms were conducted in the muscularis of postmenopausal women (Figure 7D). Although MMP-9 was increased 3.3-fold in premenopausal women with prolapse, MMP-9 was increased markedly in postmenopausal women with prolapse (23-fold; Figure 7E). Although it is possible that increased expression of MMP-9 may be associated with the increased age of our cohort of menopausal women with prolapse, we compared expression of MMP-9 in the vaginal wall by zymography in 8 menopausal controls of less than 60 years with that of 4 menopausal women with prolapse also of less than 60 years. The results indicate that MMP-9 is increased significantly in the vaginal wall of relatively young menopausal women with prolapse (37,864 ± 30,943 vs. 526 ± 260 density units; $P < 0.004$, Mann-Whitney *U*), suggesting that increased MMP-9 is related to prolapse rather than age. Transcript levels for *MMP9* were increased dramatically in the vaginal wall from 2 postmenopausal women, both of whom displayed increased levels of MMP-9 by zymography. Notably, however, increases in MMP-9 by zymography in premenopausal and 13 of 15 postmenopausal women with prolapse were not associated with increased *MMP9* mRNA. These findings suggest that, like tissues from *Fbln5*$^{-/-}$ mice, MMP-9 is regulated predominantly at the posttranscriptional level in the vaginal wall of women with prolapse and that protease activity may be a critical factor for disease progression in human POP.

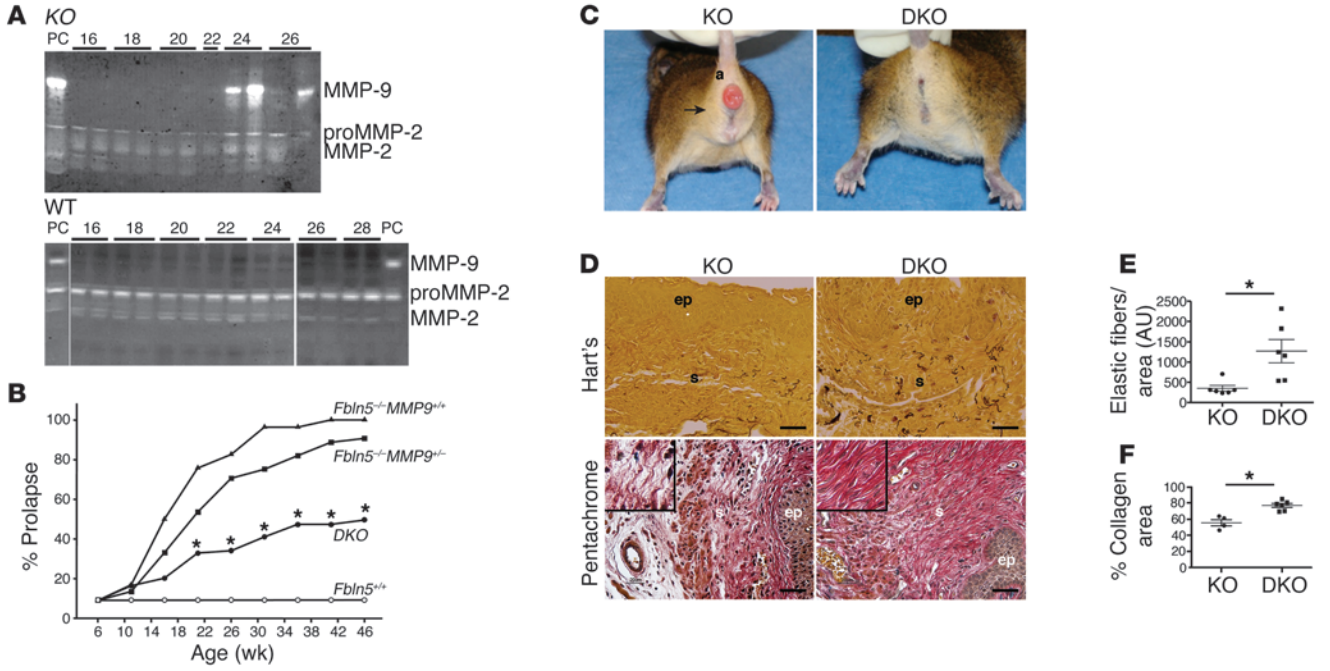

Figure 6

Attenuation of prolapse phenotypes in *Fbln5*$^{-/-}$*;Mmp9*$^{-/-}$ (DKO) mice. (**A**) Postnatal analysis of MMP-9 levels in WT and *Fbln5*$^{-/-}$ (KO) vaginas. Vaginas were harvested at indicated day and subjected to gelatin zymography. Note an increase in MMP-9 activity in the mutants at 24 days of age but not in WT. PC, adult KO vagina serves as a positive control. In WT gel, first 11 lanes were run on the same gel but were not contiguous. (**B**) Prolapse development in *Fbln5*$^{+/+}$ (n = 16–23, white circles), *Fbln5*$^{-/-}$*;Mmp9*$^{+/+}$ (n = 25–36, black triangles), *Fbln5*$^{-/-}$*;Mmp9*$^{+/-}$ (n = 39–42, black squares), and DKO (n = 18–25, black circles) from 6–46 weeks. Data represent percentage of animals developing overt prolapse (≥ stage 2). Although prolapse was assessed weekly, for simplicity, data are presented at 4-week intervals. *P < 0.01 compared with *Fbln5*$^{-/-}$*;Mmp9*$^{+/+}$ or *Fbln5*$^{-/-}$*;Mmp9*$^{+/-}$, log-rank survival analysis. (**C**) Representative images of KO (left) and DKO (right) littermates at 33 weeks. Note rescue of urogenital bulge (arrow) and anal prolapse (a) in DKO. (**D**) Representative Hart's staining (upper panels) of transverse sections of the mid-vagina from KO (n = 6) or DKO (n = 6) mice at 1 year of age. A marked increase in elastic fiber density is observed in the subepithelial stroma of DKO mice. Pentachrome staining (lower panels) of the vagina from KO (n = 3) or DKO (n = 3) mice at 1 year old. Note collagen fibrils were thicker and continuous in DKO mice compared with *Fbln5*$^{-/-}$ mice (insets). Scale bars: 20 μm. (**E**) Quantification of elastic fiber density. (**F**) Collagen area fraction. Each symbol represents mean determination from a single animal. Data are represented as mean ± SEM. *P < 0.05.

Discussion

In this study, we established a causative link between integrity of the vaginal wall and POP, which is determined by a balance between synthesis and degradation of ECM networks in the vaginal wall (Figure 8). We provided evidence that in the presence of compromised elastic fibers, MMP-9 plays a crucial role in progression of POP. We propose that fibulin-5 is a pivotal molecule with dual functions involving regulation of MMP-9 and assembly of elastic fibers in the vaginal wall. Although the RGD domain is not required for elastic fiber assembly, RGD-dependent fibulin-5–integrin interactions are critical for MMP-9 regulation, which in part involves suppression of ROS generation.

The role of integrins in the matricellular functions of fibulin-5. Initially, it was proposed that the RGD motif in fibulin-5 played a role in the final step of elastic fiber assembly by tethering polymerized elastin to surrounding cells (14, 28). Subsequent biochemical studies, however, showed that fibulin-5 preferentially binds to the monomeric form of elastin and positively regulates coacervation, but negatively regulates maturation of coacervated elastin in vitro (18, 36). Our present study provides genetic evidence that RGD-dependent integrins are not directly involved in fibulin-5–mediated elastic fiber assembly in vivo. Takahashi et al. (37) used *FN*$^{RGE/RGE}$ mutant embryos to show that the RGD motif in the FN-III domain of fibronectin (i.e., the motif that interacts with $\alpha_5\beta_1$ or $\alpha_v\beta_3$ integrins) is dispensable for assembly of fibronectin fibrils, yet this interaction is essential for vascular development. The iso-aspartate-GR motif in FN-I_5 was shown to compensate for RGD-mediated binding to integrins. Therefore, we cannot rule out the possibilities that fibulin-5 uses other region(s) to bind integrins or that an alternative cell surface receptor exists to aid in the assembly of elastic fibers in *Fbln5*$^{RGE/RGE}$ mutants.

In contrast to fibulin-5–mediated elastogenesis, fibulin-5–mediated suppression of MMP-9 is dependent on the RGD motif. These experiments thereby molecularly defined integrin-dependent and -independent functions of fibulin-5. Furthermore, our results suggest that regulation of MMP-9 through the RGD domain of fibulin-5 occurs in a tissue-specific manner. We speculate that although we did not detect upregulation of MMP-9 in quiescent adult aorta or skin of *Fbln5* mutant mice, it is possible that acute or chronic injury may induce differential upregulation of matrix protease(s), where the composition of ECM may change during pathological insults.

It was previously reported that overexpression of fibulin-5 reduced metastasis of H460 lung cancer cells by inhibiting MMP-7 (25). This inhibitory effect was dependent on RGD-integrin interactions, which resulted in inhibition of phosphorylated ERK sig-

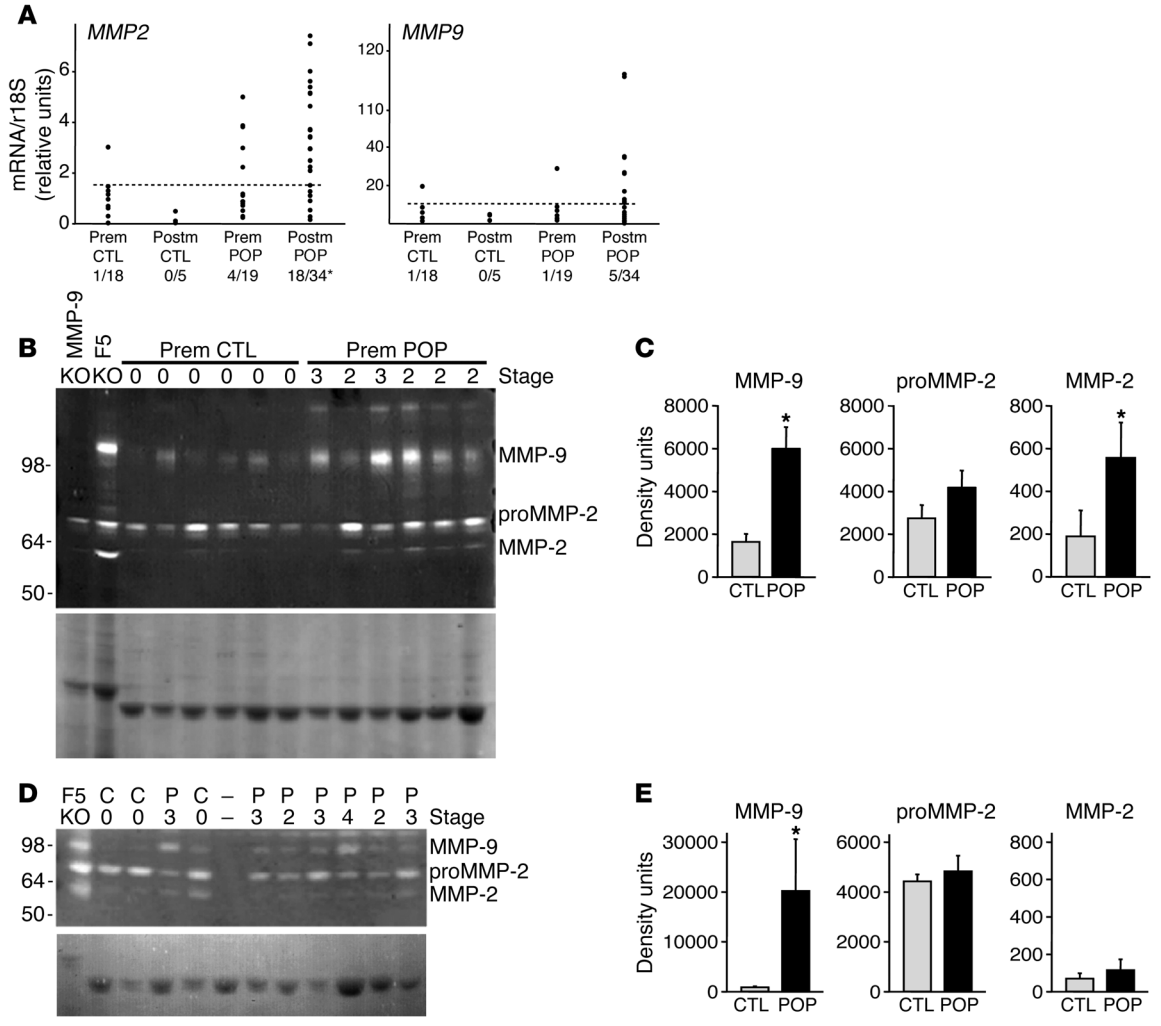

Figure 7

Increased MMP-9 activity in human POP patients. (**A**) *MMP2* and *MMP9* mRNA levels in vaginal muscularis from women with and without POP. Levels of *MMP2* (left) and *MMP9* (right) mRNA were quantified in vaginal muscularis from asymptomatic premenopausal (Prem CTL, $n = 18$) and postmenopausal (Postm CTL, $n = 5$) controls and premenopausal (Prem prolapse, $n = 19$) and postmenopausal (Postm prolapse, $n = 34$) women with POP. Dashed lines represent 95% CI of values from premenopausal controls. Each symbol represents mean determination from a single patient. *$P < 0.05$ compared with other groups, χ^2 analysis. (**B**) Gelatin zymography of vaginal muscularis from premenopausal women with (Prem prolapse) or without (Prem CTL) POP. Vaginal extracts from *Mmp9*$^{-/-}$ and *Fbln5*$^{-/-}$ mice were used as negative and positive controls. (**C**) Quantification of pro– and active MMP-2 and MMP-9 from premenopausal women with or without POP, respectively. (**D**) Representative zymogram of vaginal muscularis from postmenopausal with (P) or without (C) prolapse. Coomassie blue staining of the extracts (20 μg/lane) is shown in the lower panel as a control for protein loading. Gelatinolytic activity corresponding to MMP-9 (~105 kDa), proMMP-2 (72 kDa), and active MMP-2 (62 kDa) is seen as clear bands of lysis. Stage of prolapse is noted above each lane. 1 lane (–) was loaded on the Coomassie gel, but not the zymogram. (**E**) Quantification of proMMP-2, active MMP-2, and MMP-9 in 8 controls and 15 postmenopausal women with prolapse. *$P < 0.01$.

naling and transcriptional downregulation of MMP-7. Interestingly, the mechanisms by which fibulin-5 suppresses MMP-9 in the vaginal wall appear to be different because increases in MMP-9 in the *Fbln5*$^{-/-}$ or *Fbln5*$^{RGE/RGE}$ vagina do not involve upregulation of *Mmp9* mRNA. Fibronectin-mediated upregulation of MMP-9 has been shown to be mediated via $\alpha_5\beta_1$ integrin in vitro (23, 38). Our in vitro data show that fibronectin-mediated increases in MMP-9 (a) occurred in the absence of fibulin-5 and (b) were suppressed by fibulin-5, and (c) that fibulin-5 itself had no effect on baseline levels of MMP-9 in vaginal stromal cells. These results are consistent with previous observations in which fibulin-5 competes with fibronectin for β_1 integrin binding and binding of fibulin-5 to β_1 integrins does not lead to activation (29). We also showed that the absence of fibulin-5 enhances ROS levels in response to fibronectin in mouse embryonic fibroblasts (26). Since ROS is a known activator of proMMP-9 (39), it is conceivable that increases in ROS levels account for increases in active MMP-9 in the *Fbln5* mutant vagina. Taken together, our data suggest that fibulin-5 functions to antagonize an overall increase of pro– and active MMP-9 induced by fibronectin-integrin interactions in the vaginal wall.

Loss of homeostasis of ECM and POP in mice and humans. Vaginal tissue remodeling is a continuous process and represents a delicate balance between matrix synthesis and breakdown. This balance is necessary to maintain integrity of the tissue during reproduc-

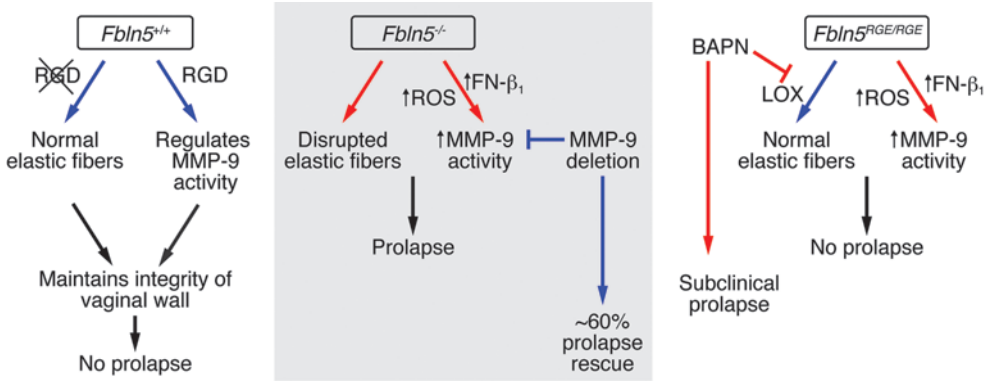

Figure 8

Schematic presentation of the dual role of fibulin-5 in prevention of POP. In WT mice, fibulin-5 controls assembly of elastic fibers (in an RGD-independent manner) and MMP-9 activity (in an RGD-dependent manner) in the vaginal wall and prevents development of POP. In the absence of fibulin-5 (*Fbln5*$^{-/-}$), elastic fibers are disrupted and MMP-9 activity is upregulated through increased fibronectin-integrin (FN-β_1) interactions and generation of ROS in vaginal stromal cells. Upregulation of MMP-9 activity is important in the pathogenesis of prolapse because deletion of MMP-9 results in significant rescue of the prolapse phenotype. In the presence of RGE mutation (*Fbln5*$^{RGE/RGE}$), upregulation of MMP-9 itself was not sufficient to cause POP due to a presence of intact elastic fibers; however, inhibition of LOX activity by BAPN together with the increased MMP-9 led to subclinical POP. Blue and red arrows indicate normal and abnormal conditions, respectively.

tive cycles and after parturition. Although *Fbln5*$^{RGE/RGE}$ female mice display a unique biochemical phenotype, these animals were rescued from prolapse development, indicating that the presence of intact elastic fibers is protective for development of POP in vivo. Inhibition of LOX activity by BAPN in *Fbln5*$^{RGE/RGE}$ mice, however, resulted in a statistically significant increase in perineal body length compared with BAPN-treated WT animals ($P < 0.01$). Since *Fbln5*$^{RGE/RGE}$ mice exhibit subclinical levels of POP phenotype without histological abnormalities, this suggests that elastic and collagen fibers synthesized prior to administration of BAPN may be sufficient to protect from matrix degradation even in the presence of elevated MMP-9. Interestingly, our studies in DKO mice indicate that abnormal elastic fibers alone are insufficient for full development of the prolapse phenotype. Rather, matrix proteases, together with abnormal elastic fibers, appear to play important roles in loss of pelvic organ support.

Alterations in the vaginal ECM are shown in women with POP, and several studies have reported increased levels of matrix metalloproteases in advanced POP (40, 41). Our observations of age-dependent worsening of prolapse in *Fbln5*$^{-/-}$ mice and marked attenuation of prolapse in the absence of MMP-9 in *Fbln5*$^{-/-}$ mice lead to the conclusion that defective elastic fiber synthesis together with proteolytic degradation of ECM plays a critical role in development of POP in vivo. Indeed, we observed marked improvement of elastic fiber density as well as collagen fiber bundles in lamina propria of the DKO vaginal wall. This indicates that progressive degradation of ECM is a deteriorating factor for prolapse in *Fbln5*$^{-/-}$ mice. Surprisingly, approximately 40% of DKO mice were not rescued from POP. Since we observed upregulation of caseinolytic serine proteases in the *Fbln5*$^{-/-}$ vagina (our unpublished observations), it is possible that matrix proteases other than MMP-9 contribute to degradation of the ECM in connective tissues of the pelvic floor. Nevertheless, our studies provide what we believe is a novel concept, that POP is an acquired matrix disease that results from disruption of the integrity of the vaginal wall, which is contiguous with its supportive connective tissue.

Therapeutic implications. Our study unexpectedly highlights the role of vaginal stromal cells, characterized by α-SM actin– and vimentin-positive cells of mesenchymal origin, in contributing to the synthesis and secretion of MMP-9 in the vaginal wall. Since (a) stromal cells express both estrogen receptor isoforms (42), (b) timing of MMP-9 induction in the *Fbln5*$^{-/-}$ vagina coincides with initiation of estrus cycling in mice, and (c) estradiol is known to induce fibronectin production in vitro (43, 44), estrogen-induced initiation of vaginal remodeling may be important in the initiation of prolapse in mice. Although upregulation of MMP-9 in *Fbln5*$^{-/-}$ vagina depends on fibronectin-integrin interactions and consequent production of ROS in the vaginal wall, it is also plausible that remodeling of the vaginal wall during estrogen withdrawal or with antiestrogen therapy may exert adverse effects through upregulation of MMP-9 (45) and loss of the antioxidant function of estrogen (46, 47). In addition, oxidative modification of elastin has been shown to reduce its binding ability to elastic fiber–associated proteins, including fibulin-4, fibulin-5, and fibrillin-2, leading to compromised elastic fiber assembly (48). Thus, MMP-9 inhibitors, together with antioxidants, may result in prevention (or amelioration) of prolapse in *Fbln5*$^{-/-}$ mice. Alternatively, strengthening of the ECM network with estrogen while controlling ROS levels by antioxidants or MMP-9 inhibitors may be effective. Our present studies provide the rationale for matrix protease–targeted therapy in women at risk for POP and warrant further investigation.

Methods

Mice. Two strains of *Fbln5*$^{-/-}$ mice were used in this study. The C18-6 line was generated as previously described (14), and 3H and 8F lines were generated by germline deletion of *Fbln5* in mice heterozygous for a conditional allele of *Fbln5* using CAG-Cre deleter transgenic mice (49), then mated to generate homozygous mice. Generation of mice carrying a conditional allele of *Fbln5* is described elsewhere. Both lines showed identical phenotypes of systemic elastic fiber defects (data not shown). *Mmp9*$^{-/-}$ mice were purchased from Jackson Laboratories (FVB.Cg-*Mmp9*^{tm1Tvu}/J) and crossed with *Fbln5*$^{+/-}$ mice to obtain double-heterozygous mice, which were subsequently intercrossed to obtain *Fbln5*$^{-/-}$;*Mmp9*$^{-/-}$ double homozygous mice (DKO). Littermates with *Fbln5*$^{-/-}$;*Mmp9*$^{+/+}$ or *Fbln5*$^{-/-}$; *Mmp9*$^{+/-}$ genotypes were used as controls in the prolapse study. Animals were assessed for POP weekly by examiners blinded to genotype. WT or heterozygous mice from the same litter were used as controls in other experiments. All mice were kept on a 12-hour light/12-hour dark cycle under specific pathogen–free conditions, and animal experimental procedures were reviewed and approved by the Institutional Animal Care and Use Committees of the University of Texas Southwestern Medical Center.

Gene targeting and genotyping. A *Fbln5RGE*-knockin vector was generated using the pGKNEO-lox2-DTA.2 vector containing a neomycin resistance cassette (Neo) flanked by loxP sites and a diphtheria toxin (DTA) gene cassette. A 3.6-kb BamHI-EcoRI fragment containing exon 4 of *Fbln5* was isolated from 129SvEv mouse Lambda FIX II library (Stratagene). D56E mutation was introduced in exon 4 by site-directed mutagenesis (QuickChange Site-Directed Mutagenesis Kit; Stratagene), and a new EcoRI site was generated downstream of exon 4. The arms contained a total of approximately 7.3 kb of homologous regions. The vector DNA was linealized with NotI and electroporated into SM-1 ES cells as previously described (50). After positive and negative selection with G418 (250 μg/ml) and DTA, 480 clones were subjected to screening by Southern blot analysis using EcoRI-digested genomic DNA hybridized with a 5′ or 3′ probe. Two ES cell clones showed correct recombination and were expanded and injected into blastocysts obtained from C57BL/6 females. Chimeras derived from each ES cell line gave germline transmission, and heterozygous mice were mated with CAG-Cre deleter transgenic mice to remove the *Neo* cassette, which resulted in generation of *Fbln5RGE* allele (*Fbln5*^{RGE}). Absence of *Neo* was confirmed by PCR (forward 5′-TATTCGGCTATGACTGGGCACAACAG-3′ and reverse 5′-TTCCACCATGATATTCGGCAAGCAGG-3′). Subsequent genotyping was performed by PCR (forward 5′-GACCTGGACCGCCAGTCAGG-3′, and reverse 5′-CCACTGTGGTTGAGATCTTCAGGATC-3′) to distinguish approximately 900-bp WT and approximately 930-bp mutant bands.

Histology and immunohistochemistry. Vaginal tissues were dissected and fixed in 4% paraformaldehyde, embedded in paraffin, and sectioned at 5-μm intervals. For cryosections, tissues were embedded in OCT and frozen in liquid N_2, and 10-μm sections were prepared. H&E staining was performed for routine histology, Hart's stain for elastic fibers, and Masson's trichrome, pentachrome, or picrosirius red stains for visualization of collagen fibers. For immunostaining on paraffin-embedded sections, tissues were deparaffinized in xylene, followed by a graded series of ethanol exchanges, and rehydrated in PBS containing 0.1% Tween (PBST). For immunostaining on cryosections, specimens were fixed in 4% paraformaldehyde/PBS or acetone for 15 minutes at room temperature (RT). Both frozen and paraffin-embedded sections were blocked in 1% BSA/2% normal goat serum (NGS) or 3% BSA in PBST for 1 hour at RT. Primary antibodies were diluted in 1% BSA/2% NGS and incubated overnight at 4°C or for 1 hour at 37°C. After washing 5 times in PBST, sections were incubated with FITC or Alexa Fluor 488–conjugated goat anti-rabbit secondary antibody (1:500, Vector Laboratories; Invitrogen) or Alexa Fluor 594–conjugated goat anti-mouse secondary antibody (1:500; Invitrogen) for 1 hour at RT. After washing with PBST, sections were mounted in Vectashield with DAPI (Vector Laboratories) and viewed using a fluorescence microscope (DMRXE; Leica). Antibodies used in this study were as follows: anti–fibulin-5 (BSYN 1923, 1:500; ref. 14) and anti-nitrotyrosine (1:500; Millipore).

Morphometric analysis. Images were captured using Leica DM2000 under identical conditions, including camera exposure and microscope illumination. Morphometric analysis was performed using ImageJ software (http://rsbweb.nih.gov/ij/) (NIH) by a blinded examiner. Elastic fiber area was assessed on Hart's stained vaginal cross sections using 4–6 images from each *Fbln5*$^{-/-}$ (n = 6) and DKO (n = 6) mouse. All sections were set to a consistent threshold limit, and the values were calculated as average elastic fiber pixel area in the vaginal stroma. For collagen fiber analysis, vaginal cross sections stained with picrosirius red were used. Three images from each *Fbln5*$^{-/-}$ (n = 4) and DKO (n = 6) mouse were analyzed. All sections were set to a consistent threshold limit, and the values were calculated as percentage of collagen pixel area over total vaginal stromal area.

Gelatin zymography. Vaginal tissues were pulverized and homogenized in Tris buffer (10 mM Tris-HCl, pH 7.4, 150 mM NaCl, 10 mM $CaCl_2$) containing 0.1% Triton-X 100. Homogenates were centrifuged at 10,000 *g* for 15 minutes at 4°C. Protein concentration in supernatants was determined using a Bradford protein assay kit (Bio-Rad). Protein samples were prepared by mixing with nonreducing sample loading buffer without boiling. Samples were electrophoretically separated in 10% SDS-polyacrylamide gels containing gelatin (1 mg/ml; Sigma-Aldrich). After separation, gels were placed in 2.5% Triton X-100 in water for 1 hour, then gelatinases were activated by overnight incubation in 50 mM Tris-HCl, pH 8.0, and 5 mM $CaCl_2$ at 37°C. Under these conditions, gelatinase activity was linear with time and protein loading. Gels were stained with 0.5% Coomassie blue R250 and then destained with a 10% acetic acid, 30% methanol solution until the gelatinolytic bands were visible.

Cell culture. Primary stromal cells were isolated from vaginal tissues harvested from P14–P21 virgin mice. After bladder, uterus, and cervix were removed, vaginal tissues were rinsed in penicillin-streptomycin solution (Invitrogen) and incubated in HEPES-trypsin solution containing collagenase (2 mg/ml; Roche) and DNase (0.3 mg/ml; Roche) at 37°C for 15 minutes. Vaginas were then cut open and the epithelium was scraped off. Remaining stromal tissues were minced and incubated in a collagenase/DNase solution for 2 hours at 37°C with gentle shaking. Cells were pelleted at 390 *g* for 3 minutes, washed in HEPES buffer 2 times, and resuspended in DMEM containing 15% FBS, 1% penicillin-streptomycin (Invitrogen). After first passage, medium was changed to DMEM containing 10% FBS (designated as P1 cells). For confirmation of the cell types, P1 stromal cells were plated in a chamber slide (Lab-TEK II, NUNC) at a density of 15,000 cells/ml and subjected to immunostaining. Cells were fixed in acetone or 4% paraformaldehyde for 10 minutes on ice or at RT, respectively, then washed in TBST (10 mM Tris-HCl, pH 7.5, 0.15 mM NaCl, and 0.1% Tween 20) for 5 minutes for 3 times and blocked with 1% BSA/2% NGS for 1 hour at RT. Cells were incubated with anti-pan cytokeratin (1:500; Sigma-Aldrich), anti–α-SM actin (1: 500; Sigma-Aldrich), anti-CD68 (1:150; Serotec), or anti-vimentin (1:500; Sigma-Aldrich) for 1 hour at 37°C and incubated with appropriate secondary antibodies, including Alexa Fluor 594–conjugated goat anti-mouse secondary antibody (1:500; Invitrogen) or Alexa Fluor 488–conjugated goat anti-rat secondary antibody (1:500; Invitrogen). After washing with PBS, sections were mounted in Vectashield with DAPI (Vector Laboratories) and viewed using a fluorescence microscope (DMRXE; Leica). P1 cells were used in gelatin zymography. Stromal cells (50,000 cell/ml) were plated in a 12-well culture dish and kept in regular media for 24 hours, then changed to 0.3 ml of serum-free media and incubated for 24 hours. 50 μg of BSA (Fisher) or fibronectin (MP Biomedicals) dissolved in PBS was added to the media and incubated for 24 hours, then 40 μl of conditioned media was collected and subjected to gelatin zymography. Stromal cells were also incubated with recombinant fibulin-5 (10 μg/ml), β_1 integrin–blocking antibody (Ha2/5, 10 μg/ml; BD Biosciences — Pharmingen), and RGD peptide (200 nM).

Immunoblot analysis. Vaginal tissues were homogenized in RIPA buffer and 10–20 μg of total protein subjected to 10% SDS-PAGE. After electrophoresis, proteins were transferred to PVDF membrane for 2 hours at 4°C. PVDF membranes were incubated with primary antibody for 1 hour at RT. Membranes were then washed with TBST 3 times. Thereafter, the blots were incubated with a horseradish peroxidase–conjugated secondary antibody (1:2500, Bio-Rad) at RT for 1 hour. The membranes were incubated with luminol chemiluminescence reagent (Santa Cruz Biotechnology Inc.). Antibodies against MMP-9 proenzyme (4 μg/ml, gift from Eunice Lee and Peter Roughley, Shriners Hospital for Children, Montreal, Quebec, Canada) and GAPDH (1:3000, Cell Signaling) were used.

Tissue acquisition and processing. Vaginal tissues were obtained from women undergoing hysterectomy for benign gynecologic conditions other than POP or stress urinary incontinence and from 53 women having pelvic reconstructive surgery for POP. After cross-clamping of the vaginal apex and removal of the uterus, a full-thickness tissue specimen was obtained from the anterior vaginal apex. For patients undergoing colpocleisis procedures, the anterior

vaginal apex was identified and a tissue specimen containing both vaginal epithelium and muscularis was removed. Women with conditions known to be associated with high metalloprotease activity (i.e., severe endometriosis/adenomyosis, rheumatoid arthritis, or cervical neoplasias) were excluded. Women with POP were staged using the POP quantification scoring system (51), and women with prolapse of the anterior compartment were used in this study. Women in the control group underwent preoperative evaluation, including a pelvic examination to evaluate for the presence of prolapse, but formal staging was not performed. Vaginal muscularis was meticulously dissected free of vaginal epithelium (surgical mucosa) and was either snap frozen in liquid N_2 or fixed in RNA-Later (Ambion Technologies). Tissues were obtained with informed consent under a protocol approved by the Institutional Review Board of the University of Texas Southwestern Medical Center. Specimens that were normally discarded as surgical waste were obtained under an exempt protocol also approved by the Institutional Review Board of the University of Texas Southwestern Medical Center.

Real-time quantitative PCR. Quantitative PCR (qPCR) was used to determine the relative levels of *Mmp9*, *Mmp2*, *Timp1*, *Timp2*, in mouse vaginal tissues of indicated genotypes or in human vaginal tissues. Mouse tissues were pulverized and homogenized in Trizol reagent (Invitrogen). RNA was isolated according to manufacturer's protocol. In the case of human tissues, tissues were minced and homogenized in 4 M guanidinium isothiocyanate buffer and layered over 5.7 M cesium chloride and centrifuged overnight at 237,000 *g* to extract RNA. RNA concentration was measured, and purity was confirmed by spectroscopy. cDNA synthesis was carried out with 2 μg of total RNA in a reaction volume of 20 μl. Each reaction contained 10 mM DTT, 0.5 mM deoxynucleotide triphosphates (dNTPs), 0.015 μg/μl random primers, 40 U RNase inhibitor (Invitrogen), and 200 U reverse transcriptase (Invitrogen). PCR reactions were carried out in an ABI Prism 7000 sequence-detection system (Applied Biosystems). The reverse transcription product from 50 ng RNA was used as template, and reaction volumes (15 μl) contained Master Mix (Applied Biosystems). Primer concentrations were 900 nM. Cycling conditions were as follows: 2 minutes at 50°C, followed by 10 minutes at 95°C; then 40 cycles of 15 seconds at 95°C, and 1 minute at 60°C. SYBR Green was used for amplicon detection. Gene expression was normalized to expression of the housekeeping gene β-2 microglobulin (*B2m*) or 18S (Applied Biosystems). A preprogrammed dissociation protocol was used after amplification to ensure that all samples exhibited a single amplicon. Levels of mRNA were determined using the ddCt method (Applied Biosystems) and expressed relative to an external calibrator present on each plate. Primer sequences are listed in Supplemental Table 5.

Administration of BAPN. Control and *Fbln5*$^{RGE/RGE}$ females were treated with LOX inhibitor BAPN (Sigma-Aldrich) (0.8% in drinking water, ad libitum) from P21 until 24 weeks of age. Perineal body length and perineal bulge height were measured weekly using an MOPQ system in a blinded manner to evaluate the progression of POP (10). At the end of 24 weeks, gross photographs were taken, and the aorta, vagina, bladder, and uterus were harvested for morphological and biochemical analysis.

Quantification of desmosine and HP. Elastic fiber content was assessed by radioimmunoassay for desmosine, an elastin-specific cross-link. Briefly, vaginal tissues were hydrolyzed in 6 N HCl at 100°C for 24 hours, and an aliquot was evaporated to dryness and dissolved in 100 μl of H_2O, then vortexed, microfuged, and assayed for desmosine (52). HP was measured to evaluate the content of collagen fibers in vaginal tissues by colorimetric assays as previously described (53).

In situ zymography. Gelatinase activity was detected by using FITC-labeled DQ gelatin (Molecular Probes). Briefly, 10-μm frozen sections were equilibrated at RT and rinsed with PBS. Specimens were overlaid with solution containing 100 μg/ml of FITC DQ gelatin in Tris buffer (50 mM Tris-HCl, pH 8.0, 5 mM $CaCl_2$) and incubated for 2 hours at 37°C. The sections were incubated in the presence of the metalloproteinase inhibitor phenanthroline (1 mM; Sigma-Aldrich). After washing with PBS, sections were mounted in Vectashield with DAPI (Vector Laboratories) and viewed using a fluorescence microscope.

ROS detection. Vaginal tissues from mice were dissected, OCT embedded, and frozen in liquid N_2. Frozen vaginal tissue sections (10 μm) were mounted on glass slides, rinsed with PBS, and incubated in 50 μl of 5 μM DHE (Molecular Probes), cover slipped, and incubated in a humidified incubator for 30 minutes at 37°C. Then slides were DAPI stained and mounted. Nuclear red fluorescence was visualized and images captured using a fluorescence microscope (DMRXE).

Electron microscopy. Aortae were harvested following cardiac perfusion and fixed in fixative (3% glutaraldehyde in 0.1 M sodium cacodylate, pH 7.4) overnight at 4°C. After extensive washing in 0.1 M sodium cacodylate buffer, the aortas were sequentially treated with osmium tetroxide, tannic acid, and uranyl acetate, then dehydrated and embedded in Epon as previously described (54). Thin sections (60 nm) were counterstained with methanolic uranyl acetate and lead citrate and viewed using a Tecnai 12 transmission electron microscope at 120 kV.

Statistics. Differences between 2 groups were determined using the 2-tailed Student's *t* test. Differences among 3 or more genotypes were assessed using ANOVA followed by Bonferroni's method for post hoc pairwise multiple comparisons. Differences in prolapse development among WT, KO, or DKO mice were determined using a log rank survival analysis. A χ^2 analysis was used to examine differences in *MMP2* and *MMP9* RNA levels in human vaginal tissues. $P < 0.05$ was considered statistically significant.

Acknowledgments

We thank Jesus Acevedo, Haolin Shi, Kristi Lynn, Sheena Shah-Simpson, Melanie Vittetiman, and the Pathology and Transgenic Core Laboratories for excellent technical assistance; John Shelton and James Richardson for assistance in evaluation of histological sections; and Jose Cabrera for graphic assistance. We also thank Eunice Lee and Peter Roughley for reagents, Rolf Brekken and Marie Burdine for discussion, and Eric Olson for critical reading of the manuscript. This work was supported in part by the NIH (R01AG028048, R01HD06482401, R01HL071157), the American Heart Association (Grant-In-Aid, 0855200F), and the Welch Foundation (I1646).

Received for publication November 2, 2010, and accepted in revised form February 9, 2011.

Address correspondence to: Hiromi Yanagisawa, Department of Molecular Biology, University of Texas Southwestern Medical Center, 5323 Harry Hines Blvd., Dallas, Texas 75390-9148, USA. Phone: 214.648.7723; Fax: 214.648.1488; E-mail: hiromi.yanagisawa@utsouthwestern.edu.

Qian Zheng's present address is: Avon Products Inc., Suffern, New York, USA.

1. Jelovsek JE, Maher C, Barber MD. Pelvic organ prolapse. *Lancet*. 2007;369(9566):1027–1038.
2. Abramowitch SD, Feola A, Jallah Z, Moalli PA. Tissue mechanics, animal models, and pelvic organ prolapse: a review. *Eur J Obstet Gynecol Reprod Biol*. 2009;144 suppl 1:S146–S158.
3. Word RA, Pathi S, Schaffer JI. Pathophysiology of pelvic organ prolapse. *Obstet Gynecol Clin North Am*. 2009;36(3):521–539.
4. Olsen AL, Smith VJ, Bergstrom JO, Colling JC, Clark AL. Epidemiology of surgically managed pelvic organ prolapse and urinary incontinence. *Obstet Gynecol*. 1997;89(4):501–506.
5. Matharu KS, et al. Toll-like receptor 4–mediated regulation of spontaneous Helicobacter–dependent

colitis in IL-10–deficient mice. *Gastroenterology*. 2009;137(4):1380–1390.
6. Rahn DD, et al. Failure of pelvic organ support in mice deficient in fibulin-3. *Am J Pathol*. 2009;174(1):206–215.
7. Drewes PG, et al. Pelvic organ prolapse in fibulin-5 knockout mice: pregnancy-induced changes in elastic fiber homeostasis in mouse vagina. *Am J Pathol*. 2007;170(2):578–589.
8. Liu X, et al. Elastic fiber homeostasis requires lysyl oxidase-like 1 protein. *Nat Genet*. 2004;36(2):178–182.
9. Connell KA, Guess MK, Chen H, Andikyan V, Bercik R, Taylor HS. HOXA11 is critical for development and maintenance of uterosacral ligaments and deficient in pelvic prolapse. *J Clin Invest*. 2008; 118(3):1050–1055.
10. Wieslander CK, et al. Quantification of pelvic organ prolapse in mice: vaginal protease activity precedes increased MOPQ scores in fibulin 5 knockout mice. *Biol Reprod*. 2009;80(3):407–414.
11. Argraves WS, Greene LM, Cooley MA, Gallagher WM. Fibulins: physiological and disease perspectives. *EMBO Rep*. 2003;4(12):1127–1131.
12. de Vega S, Iwamoto T, Yamada Y. Fibulins: multiple roles in matrix structures and tissue functions. *Cell Mol Life Sci*. 2009;66(11–12):1890–1902.
13. Yanagisawa H, Davis EC. Unraveling the mechanism of elastic fiber assembly: The roles of short fibulins. *Int J Biochem Cell Biol*. 2010;42(7):1084–1093.
14. Yanagisawa H, et al. Fibulin-5 is an elastin-binding protein essential for elastic fibre development in vivo. *Nature*. 2002;415(6868):168–171.
15. Freeman LJ, et al. Fibulin-5 interacts with fibrillin-1 molecules and microfibrils. *Biochem J*. 2005; 388(pt 1):1–5.
16. El-Hallous E, et al. Fibrillin-1 interactions with fibulins depend on the first hybrid domain and provide an adaptor function to tropoelastin. *J Biol Chem*. 2007;282(12):8935–8946.
17. Zheng Q, et al. Molecular analysis of fibulin-5 function during de novo synthesis of elastic fibers. *Mol Cell Biol*. 2007;27(3):1083–1095.
18. Hirai M, et al. Fibulin-5/DANCE has an elastogenic organizer activity that is abrogated by proteolytic cleavage in vivo. *J Cell Biol*. 2007;176(7):1061–1071.
19. Choudhury R, et al. Differential regulation of elastic fiber formation by fibulin-4 and -5. *J Biol Chem*. 2009;284(36):24553–24567.
20. Yanagisawa H, Schluterman MK, Brekken RA. Fibulin-5, an integrin-binding matricellular protein: its function in development and disease. *J Cell Commun Signal*. 2009;3(3–4):337–347.
21. Huveneers S, Truong H, Fassler R, Sonnenberg A, Danen EH. Binding of soluble fibronectin to integrin alpha5 beta1 - link to focal adhesion redistribution and contractile shape. *J Cell Sci*. 2008;121(pt 15):2452–2462.
22. Carson AE, Barker TH. Emerging concepts in engineering extracellular matrix variants for directing cell phenotype. *Regen Med*. 2009;4(4):593–600.
23. Booms P, et al. RGD-containing fibrillin-1 fragments upregulate matrix metalloproteinase expression in cell culture: a potential factor in the pathogenesis of the Marfan syndrome. *Hum Genet*. 2005;116(1–2):51–61.
24. Nakamura T, et al. DANCE, a novel secreted RGD protein expressed in developing, atherosclerotic, and balloon-injured arteries. *J Biol Chem*. 1999;274(32):22476–22483.
25. Yue W, et al. Fibulin-5 suppresses lung cancer invasion by inhibiting matrix metalloproteinase-7 expression. *Cancer Res*. 2009;69(15):6339–6346.
26. Schluterman MK, et al. Loss of fibulin-5 binding to beta1 integrins inhibits tumor growth by increasing the level of ROS. *Dis Model Mech*. 2010; 3(5–6):333–342.
27. Lee ER, Lamplugh L, Kluczyk B, Mort JS, Leblond CP. Protease analysis by neoepitope approach reveals the activation of MMP-9 is achieved proteolytically in a test tissue cartilage model involved in bone formation. *J Histochem Cytochem*. 2006;54(9):965–980.
28. Nakamura T, et al. Fibulin-5/DANCE is essential for elastogenesis in vivo. *Nature*. 2002; 415(6868):171–175.
29. Lomas AC, Mellody KT, Freeman LJ, Bax DV, Shuttleworth CA, Kielty CM. Fibulin-5 binds human smooth-muscle cells through alpha5beta1 and alpha4beta1 integrins, but does not support receptor activation. *Biochem J*. 2007;405(3):417–428.
30. Milner R, Crocker SJ, Hung S, Wang X, Frausto RF, del Zoppo GJ. Fibronectin- and vitronectin-induced microglial activation and matrix metalloproteinase-9 expression is mediated by integrins alpha5beta1 and alphavbeta5. *J Immunol*. 2007; 178(12):8158–8167.
31. Ra HJ, Parks WC. Control of matrix metalloproteinase catalytic activity. *Matrix Biol*. 2007;26(8):587–596.
32. Nguyen AD, et al. Fibulin-5 is a novel binding protein for extracellular superoxide dismutase. *Circ Res*. 2004;95(11):1067–1074.
33. Uzoma A, Farag KA. Vaginal vault prolapse. *Obstet Gynecol Int*. 2009;2009:275621.
34. Kadoya K, et al. Fibulin-5 deposition in human skin: decrease with ageing and ultraviolet B exposure and increase in solar elastosis. *Br J Dermatol*. 2005; 153(3):607–612.
35. Bruel A, Ortoft G, Oxlund H. Inhibition of cross-links in collagen is associated with reduced stiffness of the aorta in young rats. *Atherosclerosis*. 1998; 140(1):135–145.
36. Cirulis JT, et al. Fibrillins, fibulins, and matrix-associated glycoprotein modulate the kinetics and morphology of in vitro self-assembly of a recombinant elastin-like polypeptide. *Biochemistry*. 2008;47(47):12601–12613.
37. Takahashi S, et al. The RGD motif in fibronectin is essential for development but dispensable for fibril assembly. *J Cell Biol*. 2007;178(1):167–178.
38. Xie B, Laouar A, Huberman E. Fibronectin-mediated cell adhesion is required for induction of 92-kDa type IV collagenase/gelatinase (MMP-9) gene expression during macrophage differentiation. The signaling role of protein kinase C-beta. *J Biol Chem*. 1998;273(19):11576–11582.
39. Morita-Fujimura Y, Fujimura M, Gasche Y, Copin JC, Chan PH. Overexpression of copper and zinc superoxide dismutase in transgenic mice prevents the induction and activation of matrix metalloproteinases after cold injury-induced brain trauma. *J Cereb Blood Flow Metab*. 2000;20(1):130–138.
40. Moalli PA, Shand SH, Zyczynski HM, Gordy SC, Meyn LA. Remodeling of vaginal connective tissue in patients with prolapse. *Obstet Gynecol*. 2005; 106(5 pt 1):953–963.
41. Phillips CH, Anthony F, Benyon C, Monga AK. Collagen metabolism in the uterosacral ligaments and vaginal skin of women with uterine prolapse. *BJOG*. 2006;113(1):39–46.
42. Buchanan DL, Kurita T, Taylor JA, Lubahn DB, Cunha GR, Cooke PS. Role of stromal and epithelial estrogen receptors in vaginal epithelial proliferation, stratification, and cornification. *Endocrinology*. 1998;139(10):4345–4352.
43. Quinn JA, Graeber CT, Frackelton AR Jr, Kim M, Schwarzbauer JE, Filardo EJ. Coordinate regulation of estrogen-mediated fibronectin matrix assembly and epidermal growth factor receptor transactivation by the G protein-coupled receptor, GPR30. *Mol Endocrinol*. 2009;23(7):1052–1064.
44. Soldano S, et al. Effects of estrogens on extracellular matrix synthesis in cultures of human normal and scleroderma skin fibroblasts. *Ann N Y Acad Sci*. 2010; 1193:25–29.
45. Suzuki A, et al. Characterization and role of proteinases induced by estrogen-deprivation in female mouse reproductive tracts. *Reprod Toxicol*. 1996;10(2):129–135.
46. Bureau I, Gueux E, Mazur A, Rock E, Roussel AM, Rayssiguier Y. Female rats are protected against oxidative stress during copper deficiency. *J Am Coll Nutr*. 2003;22(3):239–246.
47. Urata Y, et al. 17Beta-estradiol protects against oxidative stress-induced cell death through the glutathione/glutaredoxin-dependent redox regulation of Akt in myocardiac H9c2 cells. *J Biol Chem*. 2006;281(19):13092–13102.
48. Akhtar K, et al. Oxidative and nitrosative modifications of tropoelastin prevent elastic fiber assembly in vitro. *J Biol Chem*. 2010;285(48):37396–37404.
49. Sakai K, Miyazaki J. A transgenic mouse line that retains Cre recombinase activity in mature oocytes irrespective of the cre transgene transmission. *Biochem Biophys Res Commun*. 1997;237(2):318–324.
50. Yanagisawa H, et al. Dual genetic pathways of endothelin-mediated intercellular signaling revealed by targeted disruption of endothelin converting enzyme-1 gene. *Development*. 1998;125(5):825–836.
51. Bump RC, et al. The standardization of terminology of female pelvic organ prolapse and pelvic floor dysfunction. *Am J Obstet Gynecol*. 1996;175(1):10–17.
52. Starcher B, Conrad M. A role for neutrophil elastase in the progression of solar elastosis. *Connect Tissue Res*. 1995;31(2):133–140.
53. Reddy GK, Enwemeka CS. A simplified method for the analysis of hydroxyproline in biological tissues. *Clin Biochem*. 1996;29(3):225–229.
54. Davis EC. Stability of elastin in the developing mouse aorta: a quantitative radioautographic study. *Histochemistry*. 1993;100(1):17–26.